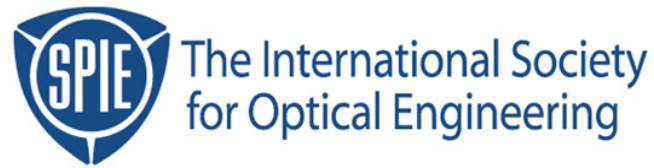


Copyright 2001 by the Society of Photo-Optical Instrumentation Engineers.



This paper was published in the proceedings of  
Advances in Resist Technology and Processing XVIII,  
SPIE Vol. 4345, pp. 1037-1047.

It is made available as an electronic reprint with permission of SPIE.

One print or electronic copy may be made for personal use only. Systematic or multiple reproduction, distribution to multiple locations via electronic or other means, duplication of any material in this paper for a fee or for commercial purposes, or modification of the content of the paper are prohibited.

# Understanding Molecular Level Effects during Post Exposure Processing

Gerard M. Schmid<sup>\*a</sup>, Mark D. Smith<sup>b</sup>, Chris A. Mack<sup>b</sup>, Vivek K. Singh<sup>c</sup>,  
Sean D. Burns<sup>a</sup>, and C. Grant Willson<sup>a</sup>

<sup>a</sup>The University of Texas at Austin, Department of Chemical Engineering, Austin, Texas, 78712;

<sup>b</sup>KLA Tencor, Corp., Austin, Texas 78759; <sup>c</sup>Intel Corporation, Hillsboro, Oregon, 97124

## ABSTRACT

The perpetual advancement of materials and equipment for microlithography has resulted in reduction of critical dimensions to scales approaching the size of the molecules that constitute a photoresist. As a result, molecular scale effects such as line edge roughness have become an increasing concern for resist manufacturers and process engineers alike. Computer simulation of lithography has become an integral tool for both process optimization and development of new technologies. However, these simulation tools are generally based upon a continuum approximation of the resist material, and are therefore unable to investigate molecular level variations. In this work we investigate the increasing importance of molecular level effects, especially in terms of the contributions of the post exposure bake (PEB) to feature roughness. A linkage has been made between a previously reported mesoscale simulation of the post exposure bake (Schmid *et al*, *Proc. SPIE – Int. Soc. Opt. Eng.*, 3999) and PROLITH® 7.0 (KLA Tencor, Corp.). The mesoscale simulation models discrete transport and reaction events during the post exposure bake to determine solubility variations on the scale of a single oligomeric chain. These solubility variations are then imported into PROLITH and transformed into photoresist topography using the familiar Mack dissolution model. This method has been used to simulate line-edge formation in an APEX®-type resist. It is found that the distribution of photoproducts produced during exposure can lead to significant solubility variations during the PEB. These solubility variations can become manifest as roughness of resist feature topography.

Keywords: PROLITH, mesoscale simulation, line-edge roughness, surface roughness

## 1. INTRODUCTION

The continued reduction in size of resist features has necessitated a concomitant reduction in error budget for critical layer feature dimension. As lithography enters the 100-nm node, aberrations in feature topography that are on the same length scale as a single resist molecule can consume a significant portion of the error budget. The increasing importance of this feature roughness has prompted researchers to devote a significant amount of effort to investigate its origins and ways to reduce it. Many factors that contribute to feature roughness have been identified, including both resist properties and processing conditions. Researchers have investigated the effect on roughness of resist properties such as molecular weight and polydispersity of resin,<sup>1,2</sup> phase separation or aggregation of resin molecules,<sup>3,4</sup> and presence of base resist additives.<sup>5,6</sup> Processing conditions have also been found to influence feature roughness, including aerial image effects,<sup>2,6,7,8</sup> bake conditions,<sup>7,9</sup> transfer of roughness from reticle,<sup>10</sup> stochastic effects that occur during dissolution,<sup>11</sup> and ultrasonic development assistance.<sup>12</sup> Feature roughness has long been a limitation of top-surface imaging techniques,<sup>13</sup> but recent work has shown that this roughness can be reduced.<sup>14,15</sup> Other researchers have investigated methods to cope with roughness by altering the perpendicular dimension of the gate to minimize the occurrence of catastrophic gate failure due to roughness.<sup>16</sup> In the work presented here, we employ lithography simulations to investigate factors that contribute to feature roughness.

### 1.1 Conventional lithography simulation

PROLITH® is one of several commercially available software packages capable of predicting resist performance as a function of the many processing variables. The first step in all these simulations is to calculate the distribution of deposited energy within the resist film that occurs during ultraviolet exposure. This is accomplished by solving Maxwell's equations for radiation propagation. The results of such calculations are very reliable because the related processing variables – exposure wavelength and resist index of refraction, for example – can be accurately measured. Furthermore, the treatment of the photoresist as a continuum material is appropriate because the length scale of diffraction during ultraviolet exposure is much larger than the length scale of the photoresist components. (Each polymer chain occupies a volume that is on the order of 5 nm in diameter.)

---

\* Electronic mail: [schmid@che.utexas.edu](mailto:schmid@che.utexas.edu). Additional information is available online at: <http://willson.cm.utexas.edu>.

The next simulation step after exposure is the post exposure bake (PEB), during which acid simultaneously moves and catalyzes reactions. Simulation of this step is generally accomplished by solving a transport equation based upon concentration-gradient-driven diffusion. Such a calculation yields the spatial distribution of acid species after the PEB, as well as the resulting solubility gradient in the polymer film. A subsequent dissolution calculation transforms the solubility gradient into photoresist topography.

### 1.2 Validity of the continuum approximation

The validity of treating the resist film as a continuum material during PEB and development simulations is arguable. In the early days of lithography simulation, the state of the art was 3 micron wide features in 1.5 micron thick novolak films. For comparison, a novolak monomer is approximately 1 nm in diameter, and the radius of gyration of a typical novolak chain is approximately 3-5 nm. These dimensions effectively define the minimum 'pixel size' of the photoresist, so the finest structure in the developed photoresist feature will be on this length scale. The effect of each individual molecule is relatively small because the component molecules are several orders of magnitude smaller than the final resist feature dimensions. Molecular level effects can be ignored in this case, and the important characteristics of the photoresist topography can be determined by using a fairly coarse calculation grid (~50 nm). On the other hand, today's lithographic techniques produce 150 nm wide features in 300 nm thick films of poly(*p*-hydroxy-co-*t*-butoxycarbonyloxy)styrene. The diameter of a resist monomer is still around 1 nm, and the radius of gyration of a typical chain is approximately 5 nm. However, the vast reduction in feature size has resulted in a situation in which individual component molecules can have a significant effect on the structure of the final photoresist feature. These effects are lost when the continuum approximation is used, on any size calculation grid.

### 1.3 Contributions to resist feature roughness

One may readily imagine how the finite size of a polymer molecule can impact the line-edge roughness of the developed photoresist feature. The situation is analogous to the case of representing an image with pixels: many small pixels are better at producing a smooth image than fewer large pixels. The difference is that developing a photoresist does not produce a gray scale. Rather, the end effect is that each polymer molecule either remains or dissolves. Ideally, this binary nature of the development process would have the effect of sharpening a smooth gradient in latent solubility. However, the solubility gradient is not smooth on the molecular level. Irregularities in the solubility gradient thus contribute to the topography of the developed resist feature.

Prior to the PEB, the polymer chains that compose the film are all ostensibly insoluble. This insolubility results from the presence of a number of blocking groups on the polymer chain. In a typical photoresist formulation, blocking 20 to 30 percent of the repeat units of a given chain is sufficient to render the chain insoluble on the time scale of the development process. Acid catalyzed thermolysis of these blocking groups takes place at the elevated temperature of the PEB. The end effect is that in regions of high acid concentration, most of the blocking groups are removed and the polymer is very soluble. Similarly, in regions of low acid concentration, most of the blocking groups remain and the polymer is insoluble. Between these two extremes lies the variation in polymer solubility that will determine the shape of the resist feature after development.

In non-chemically amplified resist processing, the purpose of the PEB is simply to remove the effect of standing waves. Each photoactive compound (PAC) can ultimately affect the solubility of a small region of the resist film; the solubility of the resist is therefore determined by the ultimate distribution of PAC molecules produced by exposure and PEB. In contrast, the effect of acid in chemically amplified resists (CARs) is cumulative over the entire PEB. The catalytic nature of the deblocking reaction allows each acid to alter the solubility of many polymer sites over a significant region of the film. Thus, while the reduction in feature size afforded by CARs has magnified the effect of individual polymer molecules, the chemical amplification has caused a simultaneous magnification in the effect of individual photoproduct molecules. For this reason, even the very small concentrations of acid that exist in the tails of aerial images can be influential in determining the shape of the developed feature.

## 2. MESOSCALE LITHOGRAPHY MODELING

Mesoscale models are models that deal with length scales between the atomistic scale and the continuum model scale. Continuum models are only strictly valid when the size of the material structure is negligible when compared to the length scale of the model. For example, these models are used in finite element simulations, where the smallest indivisible unit (the "finite element") is a purely mathematical construct and generally has no physical significance. In contrast, atomistic simulations consider individual atoms as the smallest indivisible unit. Similarly, mesoscale simulations use groups of atoms

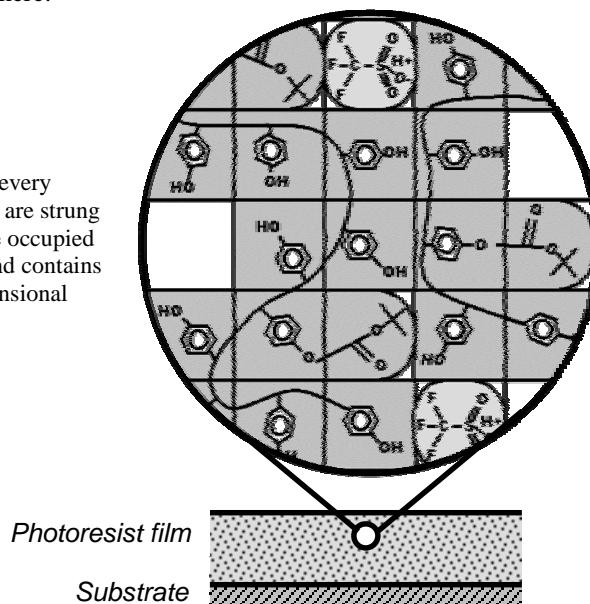
as the smallest indivisible unit. In the mesoscale simulations presented here, the smallest indivisible unit is a polymer repeat unit.

Our group has previously described mesoscale simulations of the development step.<sup>17,18</sup> Those simulations confirmed the validity of the Critical Ionization (CI) model for the dissolution of phenolic polymers in aqueous base developer, and yielded valuable insight into the influence of developer base strength and added salts on the performance of the photoresist during development. Advances continue in the simulation of the development process, and some of these advances are discussed elsewhere in these proceedings.<sup>19</sup> However, in the work presented here, the focus is on implementation of a mesoscale simulation of the PEB.

## 2.1 Mesoscale simulation framework

Our approach to molecular modeling is based upon the discretization of the photoresist film into cells on a three dimensional lattice. Each lattice cell occupies the same volume as a monomer repeat unit of the photoresist resin. Lattice cells are strung together to form oligomeric chains, and pendant groups are attached to some sites on the chains to represent the partial blocking of the photoresist resin. Some lattice cells contain PAGs and some contain photoproducts (acid plus counter-ion). Basic additives (acid quenchers), residual casting solvent, and other additives may also be included. Vacancies in the lattice represent the free volume of the polymer film. All of the lattice occupants are present in amounts that are representative of the concentrations found in the particular photoresist that is being simulated. During the simulation steps, each lattice occupant behaves in a manner consistent with its chemical identity. In this way it is possible to use the simulation to investigate the effects of the various constituents of the resist on the lithographic performance. Among the many formulation variables that may be examined in this manner are polymer molecular weight and polydispersity, PAG loading, residual casting solvent concentration, and polymer free volume. The role of acid concentration in determining resist feature topography is among the topics that will be discussed here.

Figure 1: Lattice representation of a resist film, where every molecule is considered individually. Some lattice cells are strung together to represent polymer chains and other cells are occupied by photoproducts. This example is two-dimensional and contains tens of cells. A lattice used in simulation is three-dimensional and may contain millions of cells.



### 2.1.1 Determining parameters for lattice generation

The chemical composition of the photoresist must be known before a lattice representation can be generated. Information about the resin polymer, photoacid generators, solvent, base additives (acid quenchers), and any background acid concentration must be considered. The average degree of polymerization,  $\mu_{DP}$ , as well as the standard deviation of the distribution of degree of polymerization,  $\sigma_{DP}$ , must be input. These data can be calculated from the molecular weight distribution of the photoresist resin, which is measurable using size exclusion chromatography. It is also necessary to know the average fraction of the polymer repeat units that are blocked,  $f_{BLOCK}$ , which can be determined by thermogravimetric analysis. These three variables effectively define the photoresist resin as it will be represented on the lattice. The presence of other photoresist components must also be quantified, most notably the PAG loading as a mass fraction of the polymer,  $f_{PAG}$ . The concentrations of residual casting solvent, base additives, and any background acid concentration must also be known. Techniques for measuring these quantities have been described in the literature.<sup>20,21,22</sup> Finally, a fraction of the lattice sites

are left vacant. This fraction,  $f_{\text{VOID}}$ , is produced by matching the density of the simulation lattice to the density of the actual film.

### 2.1.2 Generating a lattice representation of a resist film

Knowledge of the chemical composition of the photoresist allows one to calculate *a priori* the appropriate number population of each component in the lattice. Each component can then be added sequentially until the desired concentration is present in the lattice. In the first step of lattice creation, straight chains are added to the lattice by stringing cells together to the desired length ( $\mu_{\text{DP}}$ ) and length distribution ( $\sigma_{\text{DP}}$ ). These chains are then equilibrated via many simulated reptations that have the effect of introducing bends into the chains and eventually randomizing their conformation.<sup>23</sup> In the next step, pendant groups are added to random positions on the chains to represent blocked sites on the polymer chains. Addition of a pendant group to a chain occurs by converting a nearby lattice vacancy into a blocking unit and attaching it to the polymer at an adjacent cell. Finally, PAG molecules are added by randomly converting lattice vacancies into PAG units until the required concentration of PAG has been created. Components such as solvent and base additives can also be added at this point, but these considerations are omitted here for the sake of simplicity.

### 2.1.3 Mesoscale exposure simulation

Once the lattice is configured, it is exposed by selectively converting the PAGs into acids on the basis of their location within the photoresist film. The complexity of an exposure simulation is limitless. PROLITH 7 is capable of simulating variations in the exposure wavelength and partial coherence, the numerical aperture of the imaging system, conventional, annular, and quadrupolar illumination schemes, and arbitrary mask structures (including phase shifts), among other processing variables. The result of the exposure calculation is an energy distribution throughout the resist film, which may then be converted to the fractional conversion of PAG as a function of location within the film based upon the measured quantum efficiency of the PAG. This PAG concentration information is imported into the mesoscale simulation and the PAG species are accordingly converted into acids. DUV exposure is emphasized here, but it is also possible to perform electron beam, extreme ultraviolet (EUV), and other exposures.

### 2.1.4 Mesoscale PEB simulation

During the PEB simulation, all single-cell lattice occupants (*e.g.*, PAGs and acids) are allowed to move via a random walk through the vacant cells of the lattice. During this process, some acid molecules come into contact with blocking groups or basic additives with which they may chemically react. When an acid unit comes into contact with a blocking group it catalyzes the removal of the pendant group. In the actual resist, the volatile cleavage products generally leave the resist film in gaseous form. This reaction is modeled in the lattice simulation by removing the blocking group from the polymer chain, which temporarily leaves a void in the lattice. If the acid unit comes into contact with a base additive both units become chemically inert for the remainder of the simulation. (The effects of added base on resist performance are not explored in this work.)

## 2.2 Development model

The removal of blocking groups from the photoresist resin during the PEB causes the polymer chains to be more soluble in aqueous base developer. In the mesoscale simulation of development, the top of the lattice is exposed to developer and chains are removed if they meet the solubility criterion as defined by the Critical Ionization (CI) model. In the interest of isolating the molecular scale effects that arise during the PEB, the more familiar Mack model was used in this work to simulate the development process. This model was originally developed for use with conventional, non-chemically amplified resists, where the solubility of the film is determined by the concentration of dissolution inhibitor (PAC). In CARs, dissolution inhibition is accomplished by partially blocking the polymer chains. We therefore apply the Mack dissolution model to the spatial distribution of polymer blocking fraction after the PEB. Each location within the film is assigned the blocking fraction of the chain that occupies the associated lattice site. Sites that do not contain part of a polymer chain are assigned a value of zero because these sites will not provide any dissolution inhibition.

The Mack model dissolution rate is given by the following equation:<sup>24</sup>

$$r = r_{\text{max}} \frac{(a+1)(1-m)^n}{a+(1-m)^n} + r_{\text{min}}$$

Here, the dissolution rate  $r$  is given as a function of  $r_{\text{max}}$ , the maximum dissolution rate (corresponding to zero concentration of dissolution inhibitor),  $r_{\text{min}}$ , the lowest dissolution rate (corresponding to the maximum concentration of dissolution

inhibitor),  $m$ , the relative concentration of dissolution inhibitor, and  $n$ , a constant that describes the rate of change of dissolution rate with concentration of dissolution inhibitor. The constant  $a$  is given by the following relation:

$$a = \frac{(n+1)}{(n-1)} (1 - m_{TH})^n.$$

Here,  $m_{TH}$  is the threshold concentration of dissolution inhibitor. In the case where  $n$  is much greater than unity, the dissolution rate will change very rapidly with concentration of dissolution inhibitor in the vicinity of  $m_{TH}$ . If  $r_{min}$  is taken to be zero and a very large value of  $n$  is assumed, the resist will dissolve at the rate  $r_{max}$  in regions where  $m$  is less than  $m_{TH}$ , and will not dissolve at all in regions where  $m$  is greater than  $m_{TH}$ . This simple case is useful for separating PEB effects from dissolution effects, but actual photoresists rarely exhibit this ideal behavior.

### 3. SIMULATION RESULTS AND DISCUSSION

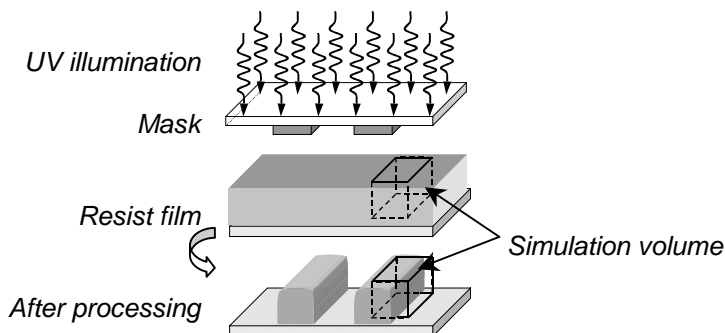
#### 3.1 Generation of a lattice model for a resist film

The results presented in this work were generated from a lattice that is 144 cells in each of the three dimensions, corresponding to a volume of approximately  $(100 \text{ nm})^3$ . This lattice was generated by adding monodisperse chains 35 repeat units long to an empty matrix and equilibrating the chains by a simulated reptation process.<sup>23</sup> In the reptation process, an entire chain may undergo snakelike motions if a void is present near one end of the chain. This process is repeated many times and has the end effect of randomizing the conformations of the chains. The mean radius of gyration, mean end-to-end distance, and the distribution of voids throughout the lattice were all monitored during the equilibration process. The lattice was considered to be at equilibrium when these lattice properties no longer changed with further equilibration steps. After equilibration, pendant groups were added to random locations on the polymer chains to represent the blocked fraction of polymer sites. The distribution of blocking fractions was Gaussian, with a mean of 0.30 and a standard deviation of approximately 0.15. Photoresists typically consist of random copolymers, so this distribution of blocking fractions is an accurate representation of what would be found in an actual resist. The last step in creating the film is to add PAG molecules to the lattice by randomly converting a fraction of the voids into PAGs. This was done such that the number ratio of polymer sites to PAG sites was 20:1, leaving ten percent of the lattice vacant to represent the available free volume in the polymer film. At this stage the lattice model accurately represents a  $(100 \text{ nm})^3$  volume of an APEX®-type photoresist film.

#### 3.1 Analysis of feature edge formation: PEB

The high sensitivity provided by chemically amplified resists is a result of the catalytic action of the photoproducts. A single acid produced during exposure can cause many reactions that will alter the solubility of the resist film. However, an acid molecule can only cause reactions if reactive material is present nearby. Each acid must therefore undergo a certain degree of translational motion in order to continue to react. In this respect, acid transport is desirable in that it allows a single photogenerated acid to alter the solubility of a larger portion of the resist film. On the other hand, transport of acid into unexposed regions of the resist film complicates control over feature dimensions.<sup>25,26</sup> To more fully understand how acid molecules near the nominal feature edge affect the final topography, we have performed several simulations of feature edges. These simulations all focus on a  $(100 \text{ nm})^3$  resist volume that is centered around the nominal feature edge of a 100 nm equal lines and spaces exposure.

Figure 2: Diagram of the simulation volume used to investigate line edge formation.



The importance of an individual acid molecule in determining the shape of the resist feature is related to the number of reactions that it catalyzes during the PEB and to the location of those reactions. As it happens, the location of an acid will strongly determine the number of reactions that it can catalyze. Consider an acid that is generated in the center of the exposed region of the resist film. Due to the high exposure in this region, a high number of PAGs will be converted into

acids, and the deprotection reaction will therefore proceed very quickly in this region. All of the reactive material (blocked sites) in this region will be rapidly depleted, and reactions in this region will cease. Now consider an acid that is generated in the tail of the aerial image. Very few acids will be present in regions of such low exposure, and so the reaction will proceed more slowly. Therefore, it is possible for an individual acid in a region of low acid concentration to continue to cause deblocking reactions long after the reaction has ceased in the regions of high acid concentration.

Another way of looking at the situation is to divide the resist resin material among the acids that are present on the basis of proximity. If the volume of resist that each acid had contact with is assumed to grow spherically, then it is easy to conceptualize that these volumes of influence will overlap quickly in regions of high acid concentration, as shown in Figure 3. In regions where acids are sparsely distributed, the volume of influence must increase considerably more before another reacted region is encountered. If the volume continues to grow spherically until the entire resist film has reacted, then the resist volume that an acid molecule has reacted with can be determined by a Voronoi analysis of the three-dimensional initial distribution of acids. This method defines the boundaries between two points as perpendicular bisectors of the lines connecting the two points. In this way, each specific point is enclosed by the region in space which it is nearer to than any of the other specified points. A two-dimensional example of this type of analysis is shown in Figure 4. It is readily apparent that there is less volume of resist available *per acid* in regions of high acid concentration. (It should be noted that the volume of acid influence will not actually grow spherically during the PEB, but rather in a more tortuous path as the acid moves through the film. The volumes have been depicted as spheres only for purposes of clarity.)

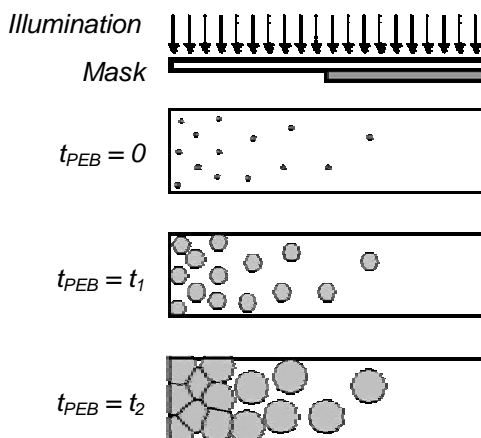


Figure 3: During the PEB, regions of acid influence quickly overlap where there are high concentrations of acid. This limits the number of reactions that each acid can participate in. An acid that is in a region of low acid concentration has much more reactive material available to it and will therefore participate in more reactions. In this two-dimensional cartoon, the region of influence has been depicted as a circle. In actuality, the acid follows a more tortuous path as it moves through the resist film.

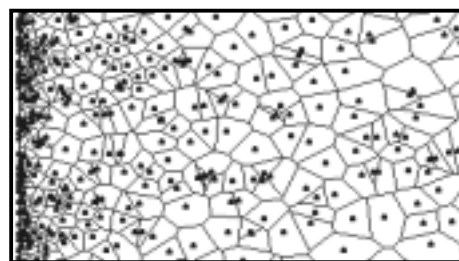


Figure 4: A two-dimensional Voronoi diagram depicting the resist area that would be influenced by each acid at the limit of complete deprotection.

To quantify this effect, simulations of line edges were performed for the exposure conditions shown in Figure 5. A step function and three sinusoids were used to simulate exposure conditions of various image slopes. PAGs in the lattice were converted to acids in accordance with the each particular exposure condition. A PEB simulation was then performed on each lattice for a total of  $5 \times 10^3$  simulation steps, during which time the number of reactions catalyzed per acid was tracked. This data has been plotted as a function of the final acid location in Figure 6. It is clear that the number of reactions that each acid catalyzes is a strong function of location for the different exposure conditions.

Figure 5: Exposure conditions used for several line edge simulations. The four cases shown represent a range of difference image slopes (IS).

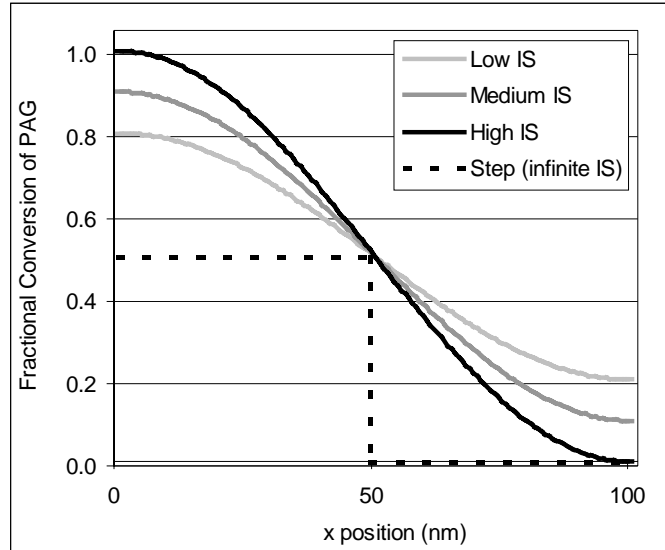
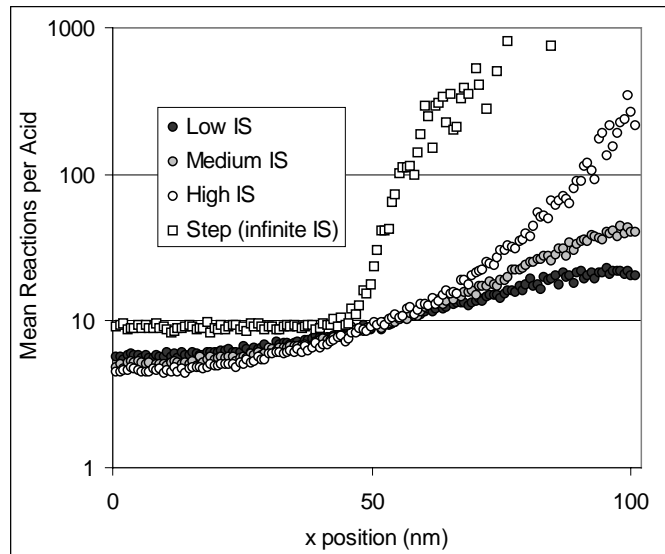


Figure 6: The mean number of reactions per acid is a strong function of location for the exposure conditions. Acids that are present in regions of low acid concentration may catalyze many more reactions than acids in regions of high acid concentration. Note the logarithmic scale on the ordinate axis.



The strong overlap of individual regions of acid influence during the PEB implies that this area of the resist is completely deprotected (or nearly so) and will dissolve quickly in the subsequent development step. These portions of the resist are not instrumental in delineating the feature edge. Rather, it is the regions where the resist has been only partially deprotected that will determine the final resist topography. To a large extent, the feature edge will occur at the interface between soluble and insoluble regions where the resin protection level has been decreased to a certain value. (This value is dependent upon both the chemical composition of the resist and the development conditions.) However, there are several ways to deprotect a resist to a given value due to the kinetics of the deprotection reaction. The same average deprotection may be produced with many acids and a short PEB or with few acids and a long PEB. The mesoscale structure of the solubility gradient is expected to be very different for the two cases.

In the next series of simulations, PAGs in the lattice were uniformly converted to several different bulk fractional conversions. A PEB simulation was performed on each lattice, and the three-dimensional solubility distribution was periodically recorded. Each solubility distribution was then inspected, and the mean and standard deviation of each was calculated. These results have been plotted in Figure 7 as the standard deviation in solubility as a function of the mean solubility for several different fractional conversions of PAG (*i.e.* different acid concentrations). The solubility of each lattice was identical prior to the PEB. During the PEB, each lattice went from higher blocking to lower blocking (right to left in Figure 7). The effect can be seen by simply plotting a slice of the solubility gradient. This has been done for two solubility distributions in Figure 8, where dark regions are more soluble than light regions. Both of these distributions have

an average blocking fraction of 0.156, but the standard deviations vary by almost a factor of 2. For equal degrees of deprotection, higher acid concentrations produce smoother gradients in solubility. These smooth gradients in solubility can be expected to produce smoother features upon development.

Figure 7: A plot of PEB-induced latent roughness. For equal degrees of deprotection, higher acid concentrations produce smoother gradients in solubility.

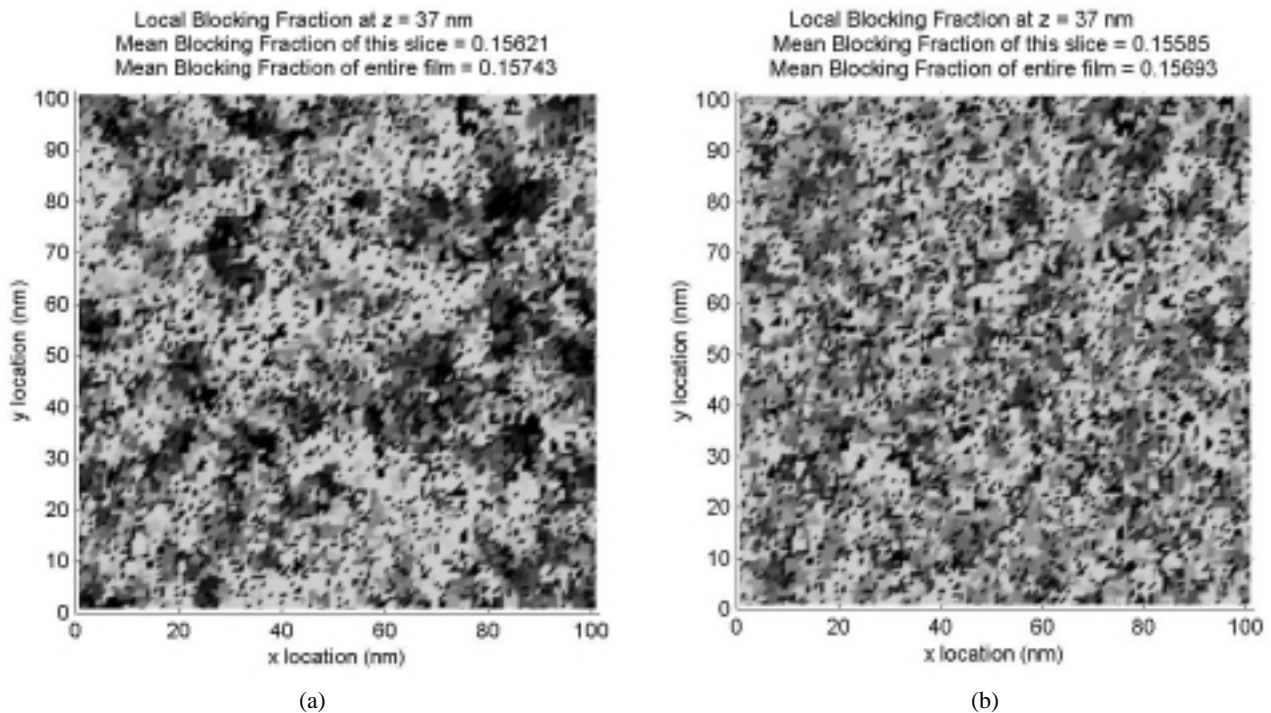
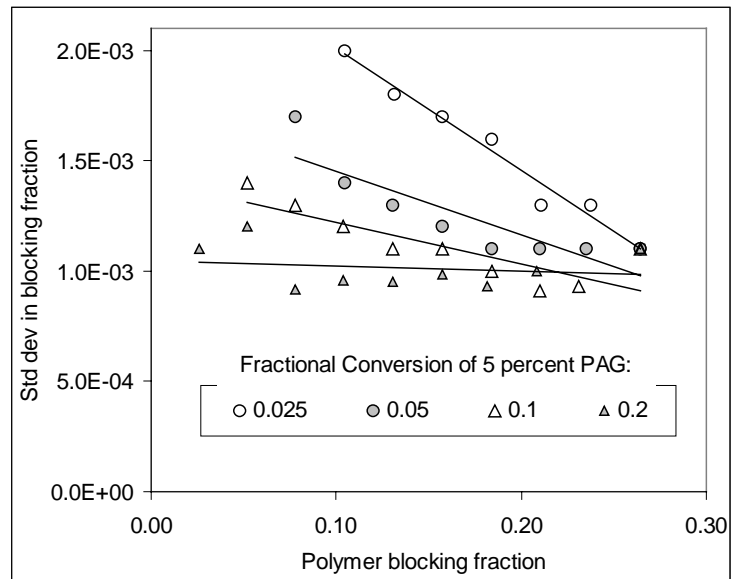


Figure 8: Slices in the solubility gradient of two lattices. Both lattices have the same average degree of deprotection, but (a) was produced with a longer PEB and fewer acids than (b). For equal degrees of deprotection, higher acid concentrations produce smoother gradients in solubility. The fractional conversion of PAG used to produce these solubility distributions was 0.025 for (a) and 0.20 for (b), resulting in standard deviations in solubility of  $1.7 \times 10^{-3}$  and  $9.8 \times 10^{-4}$ , respectively.

### 3.1 Analysis of feature edge formation: Development

The contribution of exposure and PEB to roughness can be isolated from development contributions by using a very simple threshold dissolution model. The threshold model used here is the Mack model result with zero  $r_{min}$  and infinite  $n$ , as

described in Section 2.2. The developed sidewalls that result from three of the exposure conditions from Figure 5 are shown below in Figure 9. Figure 9 (a) is the result of a step function exposure, and exhibits some molecular scale sidewall roughness (2.6 nm RMS), but little surface roughness. Figure 9 (b) is the high image slope case, and has significantly more sidewall roughness (7.0 nm RMS) and surface roughness. Figure 9 (c) is the previously defined medium image slope case. Even the relatively small decrease in image slope from (b) and (c) has noticeably increased the roughness of the feature, with the sidewall roughness increased to 11 nm RMS.

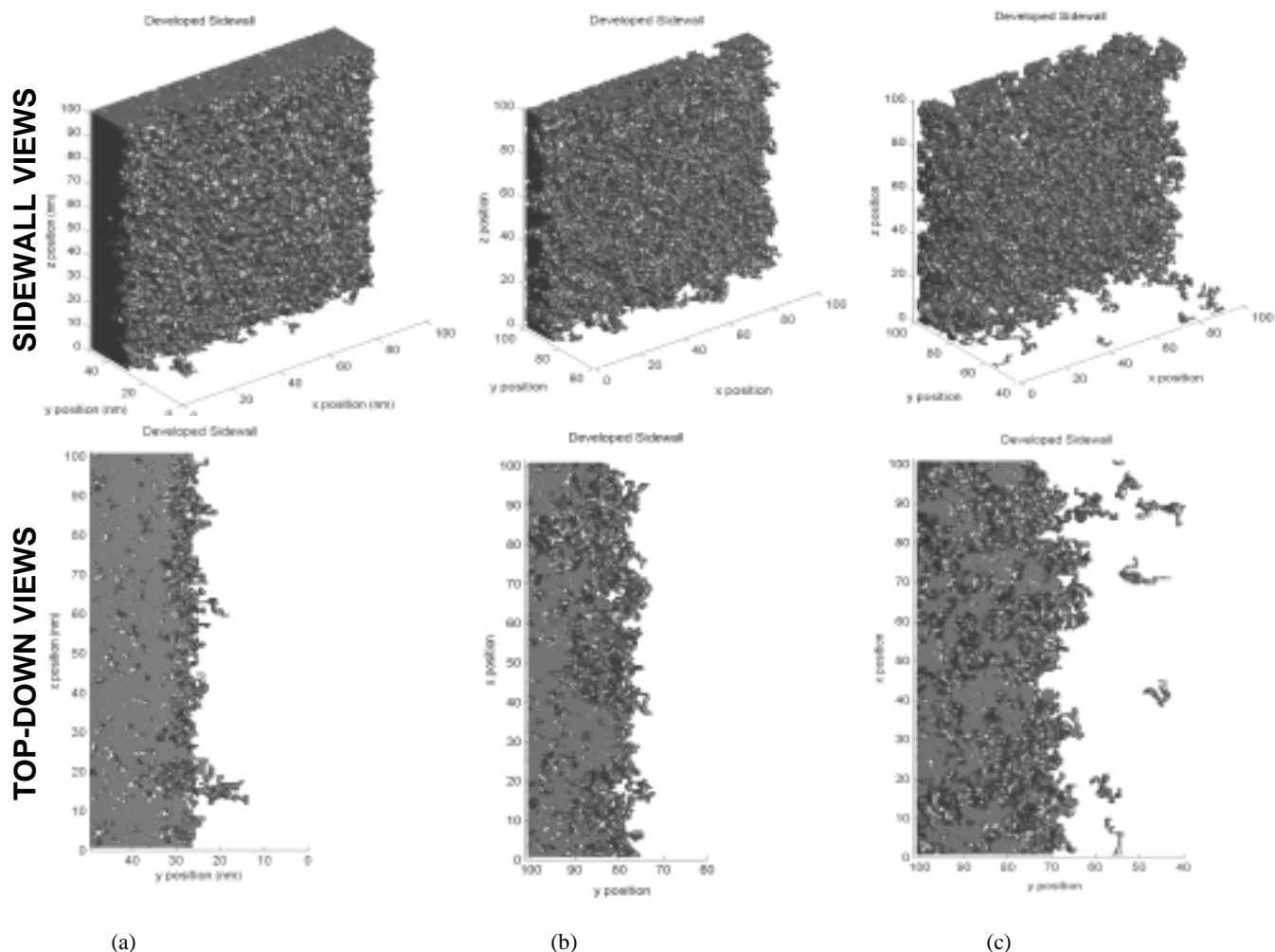


Figure 9: Line edges as developed with a simple threshold dissolution model, with  $m_{th} = 0.10$ . Both oblique (sidewall) and top-down views are shown for several different exposure conditions. The results in (a) are due to a step function exposure with infinite image slope, (b) is the result of an exposure with a high image slope, and (c) is the result of an exposure with a medium image slope, as defined in Figure 5. Outliers in the top-down views are from scumming of the substrate.

The results generated by the mesoscale model may be imported into PROLITH® as a means of performing more sophisticated dissolution algorithms. This may be done by exporting the three dimensional solubility distribution that was calculated by the mesoscale PEB model. This was done for the lattice that was produced by the step function exposure condition, and the development progress is shown in Figure 10. The three dimensional distribution of acid is defined for each point in the lattice as the blocking fraction of the polymer chain that is at that location. Thus, a single chain is represented in this construct as a continuous series of identical entries in the solubility gradient array. During threshold dissolution, these identical entries will all either remain or dissolve, so the connectivity of the chain will be preserved. Unfortunately, when using this construct with more advanced dissolution models, the connectivity of the polymer chain is not enforced, and each site will develop based upon the solubility that has been assigned to it. Future work in connecting PROLITH® to the mesoscale simulations will address these issues.

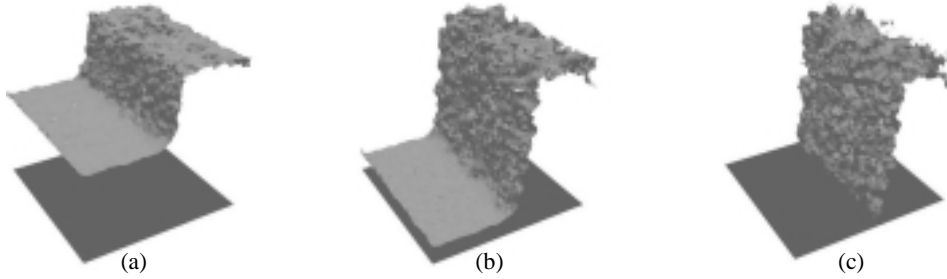


Figure 10: Development progress as simulated by Prolith® using the Mack dissolution model with  $r_{max} = 10$  nm/s,  $r_{min} = 0.1$  nm/s,  $m_{th} = 0.1$ , and  $n = 20$ . (a)  $t = 45$  s, (b)  $t = 90$  s, (c)  $t = 120$  s.

## 4. CONCLUSIONS

### 4.1 Pre-development origins of resist feature roughness

Simulations have shown that there is significant variation in the number of reactions that each acid molecule catalyzes. Acids that are in regions of high acid concentration will generally participate in far fewer reactions than acids that are in regions of low acid concentration. The feature edge will occur in a region of intermediate acid concentration. It is desirable to have this intermediate acid concentration relatively high, because simulations suggest that this will lead to a smoother solubility gradient, thereby reducing sidewall roughness. Another factor affecting sidewall roughness is the quality of the aerial image. Simulations have shown that exposures with high image slope result in reduced roughness. These results agree with the conclusions of Sanchez and coworkers at IBM,<sup>2</sup> who point out that high exposure contrast minimizes the transition region between soluble and insoluble areas of the resist film, which in turn minimizes the statistical variations in solubility that contribute to roughness.

The roughness effects that have been investigated in this work are of the extremely high-frequency variety. The size domain of the simulation is too small to allow investigation of low frequency roughness effects. Also, while the simulation allows investigation of the roughness that is generated by each molecule, this analysis is not possible through typical roughness measurements. When roughness is measured using SEM or AFM, some averaging takes place due to the resolution of the measurement. For example, AFM measurements are limited by the sharpness of the probe tip and by the lateral resolution of the instrument. Similarly, SEM measurements are strongly dependent upon the resolution of the imaging system. In addition, many SEM techniques for evaluating roughness are based upon top-down SEM measurements, which are especially susceptible to SEM image bias and sidewall averaging. A final note is that the roughness results that have been reported here were generated using a simple threshold dissolution algorithm that does not allow dangling chain ends to relax after development. This is one area of focus for future work.

### 4.2 Mesoscale models as lithography tools

The simulation framework presented here for APEX®-type resists may also be used for other resist platforms (including 193 nm and 157 nm resists), including both chemically amplified and non-chemically amplified systems. Different exposure techniques may also be considered, and this simulation technique is especially well suited for e-beam and EUV exposures, where the stochastic nature of the exposure process is important.

These simulations are quite slow. By far the slowest step is generation of an initial lattice configuration, which is especially time consuming because of the equilibration of the polymer chains. Factors affecting the length of the equilibration process include polymer DP (longer chains requiring longer equilibrations) and lattice void fraction (with higher void fractions causing a reduction in equilibration time). The lattice that was used to produce these results was produced in approximately 18 hours on a Compaq Alpha® 500 MHz workstation. However, once the lattice was made it was possible to reuse the lattice configuration as a starting point for the various exposure, PEB, and development simulations. It is only necessary to rebuild a lattice if one is interested in simulating a new resist formulation or a different volume element. It is also noteworthy that the speed of these simulations is increasing as the microelectronics industry advances because the size of photoresist features is decreasing, and the speed of computer processors is increasing.

## ACKNOWLEDGMENTS

We would like to thank Matthew Stone and Dr. Isaac Sanchez at the University of Texas at Austin for their helpful assistance and advice. This work has been supported by the SRC (Task 752.001) and DARPA. One author (GMS) gratefully acknowledges the Eastman Kodak Corporation for support in the form of a graduate research fellowship.

## REFERENCES

- <sup>1</sup> T. Yoshimura, H. Shiraishi, J. Yamamoto, and S. Okazaki, "Correlation of nano edge roughness in resist patterns with base polymers", *Jpn. J. Appl. Phys.*, **32**, pp. 6065-6070 (1993).
- <sup>2</sup> M. I. Sanchez, W. D. Hinsberg, F. A. Houle, J. A. Hoffnagle, H. Ito, and C. Nguyen, "Aerial image contrast using interferometric lithography: Effect on line-edge roughness", *Proc. SPIE – Int. Soc. Opt. Eng.*, **3678**, pp. 160-170 (1999).
- <sup>3</sup> Q. Lin, R. Sooriyakumaran, and W. Huang, "Toward controlled resist line-edge roughness: Material origin of line edge roughness in chemically amplified positive-tone resists", *Proc. SPIE – Int. Soc. Opt. Eng.*, **3999**, pp. 230-238 (2000).
- <sup>4</sup> T. Yamaguchi, H. Namatsu, M. Nagase, K. Kurihara, and Y. Kawai, "Line-edge roughness characterized by polymer aggregates in photoresists", *Proc. SPIE – Int. Soc. Opt. Eng.*, **3678**, pp. 617-624 (1999).
- <sup>5</sup> T. Ushirogouchi, K. Asakawa, M. Nakase, and A. Hongu, "Mechanism of amine additive in chemically amplified resist visualized by using Monte-Carlo simulation", *Proc. SPIE – Int. Soc. Opt. Eng.*, **2438**, pp. 609-616 (1995).
- <sup>6</sup> E. Shiobara, D. Kawamura, K. Matsunaga, T. Koike, S. Mimotogi, T. Azuma, and Y. Onishi, "Resist edge roughness with reducing pattern size", *Proc. SPIE – Int. Soc. Opt. Eng.*, **3333**, pp. 313-323 (1998).
- <sup>7</sup> S. Masuda, X. Ma, G. Noya, and G. Pawlowski, "Lithography and line-edge roughness of high activation energy resists", *Proc. SPIE – Int. Soc. Opt. Eng.*, **3999**, pp. 252-263 (2000).
- <sup>8</sup> T. Azuma, K. Chiba, M. Imabeppu, D. Kawamura, and Y. Onishi, "Line edge roughness of chemically amplified resists", *Proc. SPIE – Int. Soc. Opt. Eng.*, **3999**, pp. 264-269 (2000).
- <sup>9</sup> D. He and F. Cerrina, "Process dependence of roughness in a positive-tone chemically amplified resist", *J. Vac. Sci. Technol. B.*, **16**, pp. 3748-3751 (1998).
- <sup>10</sup> S. C. Palmateer, S. G. Cann, J. E. Curtin, S. P. Doran, L. M. Eriksen, A. R. Forte, R. R. Kunz, T. M. Lyszczarz, M. B. Stern, and C. Nelson, "Line edge roughness in sub-0.18- $\mu$ m resist patterns", *Proc. SPIE – Int. Soc. Opt. Eng.*, **3333**, pp. 634-642 (1998).
- <sup>11</sup> L. W. Flanagan, V. K. Singh, and C. G. Willson, "Surface roughness development during photoresist dissolution", *J. Vac. Sci. Technol. B.*, **17**, pp. 1371-1379 (1999).
- <sup>12</sup> S. Yasin, A. Mumtaz, D. G. Hasko, F. Carecenac, and H. Ahmed, "Characterization of the ultrasonic development process in UVIII resist", *Microelectronic Engineering*, **53**, pp. 471-474 (2000).
- <sup>13</sup> J. Hutchinson, V. Rao, G. Zhang, A. Pawloski, C. Fonseca, J. Chambers, S. Holl, S. Das, C. Henderson, and D. Wheeler, "Progress in 193 nm top surface imaging process development", *Proc. SPIE – Int. Soc. Opt. Eng.*, **3333**, pp. 165-175 (1998).
- <sup>14</sup> M. H. Somervell, D. S. Fryer, B. Osborn, K. Patterson, S. Cho, J. Byers, and C. G. Willson, "Using alicyclic polymers in top surface imaging systems to reduce line edge roughness", *Proc. SPIE – Int. Soc. Opt. Eng.*, **3999**, pp. 270-282 (2000).
- <sup>15</sup> A. T. Jamieson, M. H. Somervell, H. V. Tran, R. Hung, S. MacDonald, and C. Grant Willson, "Top surface imaging at 157 nm", *Proc. SPIE – Int. Soc. Opt. Eng.*, these proceedings (2001).
- <sup>16</sup> K. Patterson, J. L. Patterson, J. Alvis, N. Benavides, D. Bonser, N. Cave, C. Nelson-Thomas, B. Taylor, K. Turnquest, "Experimental determination of the impact of polysilicon LER on sub-100 nm transistor performance", *Proc. SPIE – Int. Soc. Opt. Eng.*, these proceedings (2001).
- <sup>17</sup> P. C. Tsiartas, L. W. Flanagan, C. L. Henderson, W. D. Hinsberg, I. C. Sanchez, R. T. Bonnecaze, and C. G. Willson, "The mechanism of phenolic polymer dissolution: A new perspective", *Macromolecules*, **30**, pp. 4656-4664 (1997).
- <sup>18</sup> L. W. Flanagan, C. L. McAdams, W. D. Hinsberg, I. C. Sanchez, and C. G. Willson, "Mechanism of phenolic polymer dissolution: Importance of acid-base equilibria", *Macromolecules*, **32**, pp. 5337-5343 (1999).
- <sup>19</sup> S. D. Burns, A. B. Gardiner, V. J. Krukoni, P. M. Wetmore, J. Lutkenhaus, G. M. Schmid, L. W. Flanagan, and C. G. Willson, "Understanding nonlinear dissolution rates in photoresists", *Proc. SPIE – Int. Soc. Opt. Eng.*, these proceedings (2001).
- <sup>20</sup> C. R. Szmanda, R. Kavanagh, J. Bohland, J. Cameron, P. Trefonas, and R. Blacksmith, "Simple method for measuring acid generation quantum efficiency at 193 nm", *Proc. SPIE-Int. Soc. Opt. Eng.* **3678**, pp.857-866 (1999).
- <sup>21</sup> A. B. Gardiner, A. Qin, C. L. Henderson, S. Pancholi, W. J. Koros, C. G. Willson, R. R. Dammel, C. A. Mack, W. D. Hinsberg, "Diffusivity measurements in polymers. II. Residual casting solvent measurement by liquid scintillation counting", *Proc. SPIE-Int. Soc. Opt. Eng.*, **3049**, pp.850-860 (1997).
- <sup>22</sup> J. F. Cameron, J. Mori, T. M. Zydowsky, D. Kang, R. Sinta, M. King, J. Scaiano, G. Pohlars, S. Virdee, T. Connolly, "Photoacid generation in chemically amplified resists: elucidation of structural effects of photoacid generators using new acid sensitive dyes for monitoring acid generation", *Proc. SPIE-Int. Soc. Opt. Eng.*, **3333**, pp. 680-691 (1998).
- <sup>23</sup> G. M. Schmid, V. K. Singh, L. W. Flanagan, M. D. Stewart, S. D. Burns, and C. G. Willson, "Recent advances in a molecular level lithography simulation", *Proc. SPIE-Int. Soc. Opt. Eng.*, **3999**, pp.675-685 (2000).
- <sup>24</sup> C. A. Mack "Development of positive photoresists", *Journal of the Electrochemical Society*, **134**, pp.148-152 (1987).
- <sup>25</sup> S. V. Postnikov, M. D. Stewart, H. V. Tran, M. A. Nierode, D. R. Medeiros, T. Cao, J. Byers, S. E. Webber, and C. G. Willson, "Study of resolution limits due to intrinsic bias in chemically amplified resists", *J. Vac. Sci. Technol. B.*, **17**, pp. 3335-3338 (1999).
- <sup>26</sup> J. Sturtevant, S. Holmes, and P. Rabidoux, "Post-exposure bake characteristics of a chemically amplified deep-ultraviolet resist", *Proc. SPIE – Int. Soc. Opt. Eng.*, **1672**, pp. 114-124 (1992).